Geometric Optimal Controls for Flapping Wing UAV on a Lie Group*

Tejaswi K. C.* Taeyoung Lee*

* The George Washington University, Washington DC 20052 (e-mail: kctejaswi999@qmail.com, tylee@qwu.edu).

Abstract: Inspired by flight characteristics captured from live Monarch butterflies, an optimal control problem is presented while accounting the effects of low-frequency flapping and abdomen undulation. A flapping-wing aerial vehicle is modeled as an articulated rigid body, and its dynamics are developed according to Lagrangian mechanics on an abstract Lie group. This provides an elegant, global formulation of the dynamics for flapping-wing aerial vehicles, avoiding complexities and singularities associated with local coordinates. This is utilized to identify an optimal periodic motion that minimizes energy variations, and an optimal control is formulated to stabilize the periodic motion. Furthermore, the outcome of this paper can be applied to optimal control for any Lagrangian system on a Lie group with a configuration-dependent inertia.

Keywords: Lagrangian mechanics, geometric mechanics, Lie group, flapping-wing unmanned aerial vehicle, optimization

1. INTRODUCTION

Millions of Monarch butterflies migrates from North America to the central Mexico during the fall, exhibiting the longest flight range among the insects (Gibo [1981]). Their dynamics are distinct from small insects, as the relatively large wings are flapping at a lower frequency, with active undulation of its abdomen. It has been suggested that abdomen undulation may reduce power consumption from the dynamic coupling of wing-body motion by Sridhar et al. [2019]. It is further reported in Dyhr et al. [2013] that moths actively modulate their body shape to control flight in response to visual pitch stimuli, and it may contribute to pitch stability. However, it is challenging to dynamically model such effects to utilize in control system design.

Flapping wing aerial vehicles are essentially infinite dimensional, nonlinear time-varying systems, where the equations of motion describing displacement and the deformation of a flexible multi-body system are coupled with the Navier-Stokes equations. Various control system design techniques have been reviewed by Shyy et al. [2016]. Most of these control systems are based on the common simplified formulation where the nonlinear time-varying flapping dynamics are transformed into linear time-invariant systems by considering small perturbations averaged over the period of flapping (see, for example, Xinyan Deng et al. [2006]). As such, these approaches are not suitable to analyze the low-frequency flapping dynamics of Monarch butterflies.

Recently, a flapping wing aerial vehicle is modeled as an articulated rigid body by Sridhar et al. [2020], where four rigid bodies representing two wings, thorax, and abdomen are interconnected via spherical joints, with the assumption of quasi-aerodynamics. The resulting dynamics are

considered as a Lagrangian system on a Lie group, and an intrinsic form of equations of motion are constructed. Compared with developing equations of motion of multirigid body systems with local coordinates, such as Euler angles, this provides an elegant, global formulation that is free of singularities. As such, this is particularly useful to design control systems inspired by Monarch. For example, it has been utilized to study the effect of abdomen undulation in energy efficiency by Tejaswi et al. [2020].

In this paper, we present an optimal control problem to stabilize a periodic motion representing the hovering flight. The flapping motion of both wings are parameterized by several variables characterizing the amplitude and the shape of oscillations, which are optimized over the numerical solutions of the aforementioned Lagrangian system. Compared with various prior works in the control of flapping wing aerial vehicles, the unique contribution is that we consider the complete dynamics involving the motion of wings, thorax, and abdomen coupled though arbitrary three-dimensional rotations and translations. In other words, the dynamics are not simplified by the common assumptions such as the longitudinal motion confined to a two-dimensional space, or the wing flapping decoupled from the body and the abdomen. These features are particularly useful to grasp the unique dynamic characteristics of Monarch, and to take the advantage of those in control system design. In short, we exploit the geometric formulation of Lagrangian mechanics on a Lie group for optimal control of a complex system inspired by Monarch. More detailed mathematical developments of this paper are available in Tejaswi and Lee [2021].

2. LAGRANGIAN MECHANICS FORMULATED ON A LIE GROUP

Consider an n-dimensional Lie group G. Let \mathfrak{g} be the associated Lie algebra, or the tangent space at the identity,

 $^{^\}star$ This research has been supported in part by NSF under the grants NSF CMMI-1761618 and CMMI-1760928.

i.e., $\mathfrak{g} = \mathsf{T}_e\mathsf{G}$. Consider a left trivialization of the tangent bundle of the group $\mathsf{TG} \simeq \mathsf{G} \times \mathfrak{g}, \ (g,\dot{g}) \mapsto (g,\mathsf{L}_{g^{-1}}\dot{g}) \equiv (g,\xi)$. More specifically, let $\mathsf{L}: \mathsf{G} \times \mathsf{G} \to \mathsf{G}$ be the left action defined such that $\mathsf{L}_g h = gh$ for $g,h \in \mathsf{G}$. Then the left trivialization is a map $(g,\dot{g}) \mapsto (g,\mathsf{L}_{g^{-1}}\dot{g}) \equiv (g,\xi)$, where $\xi \in \mathfrak{g}$. Further, suppose \mathfrak{g} is equipped with an inner product $\langle \cdot, \cdot \rangle$, which induces an inner product on $\mathsf{T}_g\mathsf{G}$ via left trivialization. For any $v,w \in \mathsf{T}_g\mathsf{G}, \langle w,v \rangle_{\mathsf{T}_g\mathsf{G}} = \langle \mathsf{T}_g\mathsf{L}_{g^{-1}}v, \mathsf{T}_g\mathsf{L}_{g^{-1}}w \rangle_{\mathfrak{g}}$. Given the inner product, we identify $\mathfrak{g} \simeq \mathfrak{g}^*$ and $\mathsf{T}_g\mathsf{G} \simeq \mathsf{T}_g^*\mathsf{G} \simeq G \times \mathfrak{g}^*$ via the Riesz representation. Throughout this paper, the pairing is also denoted by $\mathsf{Ad}_g: \mathfrak{g} \to \mathfrak{g}$, and the ad operator is denoted by $\mathsf{Ad}_g: \mathfrak{g} \to \mathfrak{g}$, and the ad operator is denoted by $\mathsf{Ad}_g: \mathfrak{g} \to \mathfrak{g}$. See, for example Marsden and Ratiu [1999] for detailed preliminaries.

We develop Euler–Lagrange equations for an arbitrary Lie group G, which are utilized later for the flapping wing UAV.

Assumption 1. The Lagrangian $L: \mathsf{G} \times \mathfrak{g} \to \mathbb{R}$ is given by the difference between kinetic and potential energy as

$$L(g,\xi) = \frac{1}{2} \langle \mathbf{J}_g(\xi), \xi \rangle - U(g), \tag{1}$$

for a configuration-dependent inertia $\mathbf{J}:\mathsf{G}\times\mathfrak{g}\to\mathfrak{g}^*$ and potential $U:\mathsf{G}\to\mathbb{R}$. Here, the inertia is a symmetric, positive-definite tensor dependent on the group.

Definition 2. The left-trivialized derivative of $\mathbf{J}_g(\xi)$ with respect to g is defined as $\mathbf{K}_q(\xi)(\cdot): \mathsf{G} \times \mathfrak{g} \to \mathfrak{g}^*$ given by

$$\mathbf{K}_{q}(\xi)\chi = \mathsf{T}_{e}^{*}\mathsf{L}_{q}(\mathbf{D}_{q}\mathbf{J}_{q}(\xi)) \cdot \chi. \tag{2}$$

along the direction $\chi \in \mathfrak{g}$. By selecting a basis of \mathfrak{g} , $\mathbf{K}_g(\xi)$ can be represented by a matrix since it is a linear operator.

The Euler-Lagrange equations for an arbitrary Lagrangian on a Lie group has been reported, for exampled by Lee et al. [2018]. Here we present a special case, when the Lagrangian is given by the configuration-dependent kinetic energy and the potential as in (1).

Theorem 3. The forced Euler-Lagrange equations corresponding to the Lagrangian in (1) are given by

$$\mathbf{J}_{g}(\dot{\xi}) + \mathbf{K}_{g}(\xi)\xi - \operatorname{ad}_{\xi}^{*}\mathbf{J}_{g}(\xi) - \frac{1}{2}\mathbf{K}_{g}^{*}(\xi)\xi + \mathsf{T}_{e}^{*}\mathsf{L}_{g}(\mathbf{D}_{g}U(g)) = f,$$
(3)
$$\dot{g} = g\xi,$$
(4)

with $f:[t_0,t_f]\to \mathfrak{g}^*$ as the generalized force acting on the system.

Proof. See Tejaswi and Lee [2021].

3. DYNAMICS OF FLAPPING WING UAV

In this section, we present a multibody model for an FWUAV, and we derive the corresponding Euler-Lagrange equations. The three-dimensional special orthogonal group is denoted by $\mathsf{SO}(3) = \{R \in \mathbb{R}^{3\times 3} \mid R^TR = I, \det(R) = 1\}$, and the corresponding Lie algebra is $\mathfrak{so}(3) = \{A \in \mathbb{R}^{3\times 3} \mid A = -A^T\}$. The Hat map $\wedge : \mathbb{R}^3 \to \mathfrak{so}(3)$ is defined such that $\hat{x}y = x \times y$ for any $x, y \in \mathbb{R}^3$. And its inverse map is the vee map, $\vee : \mathfrak{so}(3) \to \mathbb{R}^3$. Next, $e_i \in \mathbb{R}^n$ denotes the i-th standard basis of \mathbb{R}^n for an appropriate dimension n, e.g., $e_1 = (1, 0, \dots, 0) \in \mathbb{R}^n$. Throughout this paper, units are in kg, m, s, and rad, unless specified otherwise.

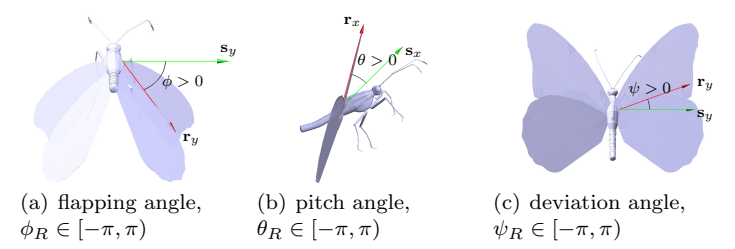


Fig. 1. Euler angles (Sridhar et al. [2020]) : positive values are indicated from \mathcal{F}_S (green) to \mathcal{F}_R (red)

3.1 Multibody Model

Let the inertial frame which is compatible to the standard north-east-down (NED) frame be $\mathcal{F}_I = \{\mathbf{i}_x, \mathbf{i}_y, \mathbf{i}_z\}$. We model the FWUAV as an articulated structure which is composed of multiple rigid bodies listed below:

- Body: This corresponds to the head and thorax combined into a single rigid body. We define $\mathcal{F}_B = \{\mathbf{b}_x, \mathbf{b}_y, \mathbf{b}_z\}$ as the body-fixed frame located at the center of mass of the body. This position is denoted by $x \in \mathbb{R}^3$ in \mathcal{F}_I , and the attitude of \mathcal{F}_B is given by $R \in SO(3)$. With $\Omega \in \mathbb{R}^3$ as the angular velocity of the body resolved in \mathcal{F}_B , the attitude evolves as $\dot{R} = R\hat{\Omega}$.
- Right wing: It is directly attached to the body. Also, we do not distinguish forewings and hindwings in our model. Let $\mathcal{F}_R = \{\mathbf{r}_x, \mathbf{r}_y, \mathbf{r}_z\}$ be the frame fixed to the right wing at its root. It is located at a constant $\mu_R \in \mathbb{R}^3$ from the origin of \mathcal{F}_B . Next, we define $\mathcal{F}_S = \{\mathbf{s}_x, \mathbf{s}_y, \mathbf{s}_z\}$ as the stroke frame obtained by translating the origin of \mathcal{F}_B to the center of wing roots, and rotating it about \mathbf{b}_y by a fixed angle $\beta \in [-\pi, \pi)$. The attitude of the right wing frame with respect to \mathcal{F}_S is denoted by 1–3–2 Euler angles $(\phi_R(t), \psi_R(t), \theta_R(t))$ (see Figure 1). So the attitude of \mathcal{F}_R relative to \mathcal{F}_B , $Q_R \in SO(3)$, can be expressed as $Q_R = \exp(\beta \hat{e}_2) \exp(\phi_R \hat{e}_1) \exp(-\psi_R \hat{e}_3) \exp(\theta_R \hat{e}_2)$, and its time-derivative will be $\dot{Q}_R = Q_R \hat{\Omega}_R$ for $\Omega_R \in \mathbb{R}^3$.
- Left Wing: The left wing frame $\mathcal{F}_L = \{\mathbf{l}_x, \mathbf{l}_y, \mathbf{l}_z\}$ is defined symmetrically to the right wing, and is located at $\mu_L \in \mathbb{R}^3$ from the origin of \mathcal{F}_B . So its attitude is, $Q_L = \exp(\beta \hat{e}_2) \exp(-\phi_L \hat{e}_1) \exp(\psi_L \hat{e}_3) \exp(\theta_L \hat{e}_2)$, with the set of Euler-angles $(\phi_L(t), \psi_L(t), \theta_L(t))$, and $\dot{Q}_L = Q_L \hat{\Omega}_L$ for $\Omega_L \in \mathbb{R}^3$.
- Abdomen: Finally, the abdomen is connected to the body via a spherical joint at which $\mathcal{F}_A = \{\mathbf{a}_x, \mathbf{a}_y, \mathbf{a}_z\}$ is attached. It is located at $\mu_A \in \mathbb{R}^3$ from origin of \mathcal{F}_B , and its attitude relative to the body is denoted by $Q_A \in \mathsf{SO}(3)$ with $\dot{Q}_A = Q_A \hat{\Omega}_A$ for $\Omega_A \in \mathbb{R}^3$.

3.2 Lagrangian Mechanics of FWUAV

The configuration of the presented model is described by $g = (x, R, Q_R, Q_L, Q_A)$ that belongs to the 15-dimensional Lie group $\mathsf{G} = \mathbb{R}^3 \times \mathsf{SO(3)}^4$. The corresponding left trivialized velocity is $\xi = (\dot{x}, \Omega, \Omega_R, \Omega_L, \Omega_A)$ which is an element of the Lie algebra, $\mathfrak{g} = \mathbb{R}^3 \times \mathfrak{so}(3)^4 \simeq \mathbb{R}^3 \times (\mathbb{R}^3)^4$.

Proposition 4. The Euler-Lagrange equations for the flapping wing UAV are given according to (3) as

$$\mathbf{J}_g(\dot{\xi}) - \mathrm{ad}_{\xi}^* \cdot \mathbf{J}_g(\xi) + \mathbf{L}_g(\xi)\xi = \mathbf{f}_a + \mathbf{f}_g + \mathbf{f}_{\tau}.$$
 (5)
Here, effects of the configuration dependent inertia is represented by the matrix $\mathbf{L}_g(\xi) = \mathbf{K}_g(\xi) - \frac{1}{2}\mathbf{K}_g^T(\xi) \in \mathbb{R}^{15 \times 15}$. Meanwhile, $\mathbf{f}_g = -\mathbf{T}_e^* \mathbf{L}_g \mathbf{D}_g U$ is the contribution of potential energy and $\mathbf{f}_a + \mathbf{f}_{\tau}$ is the non-conservative external force. The complete derivation along with detailed expressions is available in Tejaswi and Lee [2021].

4. OPTIMAL CONTROL

In this section, we present optimal controls of flapping wing UAV inspired by Monarch. First, the equations are reorganized such that the flapping motion can be described by wing kinematics. Second, we formulate an optimization to identify a periodic motion corresponding to hovering, with an additional numerical analysis to illustrate the effects of abdomen undulation. Next, we present an optimal control problem to stabilize the hovering flight.

4.1 Reduced Equations

We are interested in the global motion of the flapping wing UAV in 3-D space which is influenced by the coupled movement of wings and abdomen. So, in this section we consider a simpler case of the dynamics wherein we prescribe the motion of wings and abdomen. That is, we obtain equations governing the evolution of (x, R) for given functions $Q_R(t), Q_L(t), Q_A(t)$. This is reasonable as the inertia of the wing and the abdomen are relatively small, and the corresponding torques at the joint can be reconstructed by dynamic inversion. This corresponds to a specific choice to formulate the maneuver with wing kinematics, and the effects of dynamic coupling are still accounted completely by (5).

Definition 5. The configuration variables are decomposed into the free part and the prescribed part as

$$g_1 = (x, R), \quad \xi_1 = [\dot{x}, \Omega],$$
 (6)

$$g_2 = (Q_R, Q_L, Q_A), \quad \xi_2 = [\Omega_R, \Omega_L, \Omega_A].$$
 (7)

with $g = (g_1, g_2)$ and $\xi = (\xi_1, \xi_2)$.

Definition 6. (Configuration subspaces). Decompose all 15×15 matrices into $\{(6\times 6), (6\times 9), (9\times 6), (9\times 9)\}$ blocks. For instance, \mathbf{J}_g can be decomposed into $\mathbf{J}_{11} \in \mathbb{R}^{6\times 6}$, $\mathbf{J}_{21} \in \mathbb{R}^{9\times 6}$ and so on. Similarly a vector $\mathbf{f} \in \mathbb{R}^{15}$ can be divided into $\mathbf{f}_1 \in \mathbb{R}^6$ and $\mathbf{f}_2 \in \mathbb{R}^9$.

Proposition 7. The derivative of ξ_1 for given $(g_2, \xi_2, \dot{\xi}_2)$ can be evaluated as

$$\dot{\xi}_{1} = (\mathbf{J}_{11} - C\mathbf{J}_{21})^{-1} \left[(\operatorname{ad}_{\xi_{1}}^{*} \mathbf{J}_{11} - C\operatorname{ad}_{\xi_{2}}^{*} \mathbf{J}_{21}) \xi_{1} \right. \\
\left. - (\mathbf{L}_{11} - C\mathbf{L}_{21}) \xi_{1} - (\mathbf{J}_{12} - C\mathbf{J}_{22}) \dot{\xi}_{2} \right. \\
\left. + (\operatorname{ad}_{\xi_{1}}^{*} \mathbf{J}_{12} - C\operatorname{ad}_{\xi_{2}}^{*} \mathbf{J}_{22}) \xi_{2} - (\mathbf{L}_{12} - C\mathbf{L}_{22}) \xi_{2} \right. \\
\left. + \mathbf{f}_{a_{1}} + \mathbf{f}_{g_{1}} - C(\mathbf{f}_{a_{2}} + \mathbf{f}_{g_{2}}) \right], \tag{8}$$

where,

$$C = \begin{bmatrix} 0 & 0 & 0 \\ -Q_R & -Q_L & -Q_A \end{bmatrix} \in \mathbb{R}^{6 \times 9}.$$

Proof. The Euler–Lagrange equations (5) for the full configuration can be decomposed into two parts as

$$\mathbf{J}_{11}\dot{\xi}_1 + \mathbf{J}_{12}\dot{\xi}_2 - \mathrm{ad}_{\xi_1}^* \cdot (\mathbf{J}_{11}\xi_1 + \mathbf{J}_{12}\xi_2) +$$

$$\mathbf{L}_{11}\xi_{1} + \mathbf{L}_{12}\xi_{2} = \mathbf{f}_{a_{1}} + \mathbf{f}_{g_{1}} + \mathbf{f}_{\tau_{1}}, \qquad (9)$$

$$\mathbf{J}_{21}\dot{\xi}_{1} + \mathbf{J}_{22}\dot{\xi}_{2} - \operatorname{ad}_{\xi_{2}}^{*} \cdot (\mathbf{J}_{21}\xi_{1} + \mathbf{J}_{22}\xi_{2}) +$$

$$\mathbf{L}_{21}\xi_{1} + \mathbf{L}_{22}\xi_{2} = \mathbf{f}_{a_{2}} + \mathbf{f}_{g_{2}} + \mathbf{f}_{\tau_{2}}. \qquad (10)$$

Here the external control torques (τ_R, τ_L, τ_A) are unknown since we are directly specifying the wing and abdomen configuration. However, the above two equations are coupled by these torques through the relation, $\mathbf{f}_{\tau_1} = C\mathbf{f}_{\tau_2}$ (see Tejaswi and Lee [2021]). To remove these terms, we calculate (9) - $C \times$ (10) to obtain

$$(\mathbf{J}_{11} - C\mathbf{J}_{21})\dot{\xi}_{1} - (\mathrm{ad}_{\xi_{1}}^{*}\mathbf{J}_{11} - C\mathrm{ad}_{\xi_{2}}^{*}\mathbf{J}_{21})\xi_{1} + (\mathbf{L}_{11} - C\mathbf{L}_{21})\xi_{1}$$

$$= -(\mathbf{J}_{12} - C\mathbf{J}_{22})\dot{\xi}_{2} + (\mathrm{ad}_{\xi_{1}}^{*}\mathbf{J}_{12} - C\mathrm{ad}_{\xi_{2}}^{*}\mathbf{J}_{22})\xi_{2}$$

$$- (\mathbf{L}_{12} - C\mathbf{L}_{22})\xi_{2} + \mathbf{f}_{a_{1}} + \mathbf{f}_{g_{1}} - C(\mathbf{f}_{a_{2}} + \mathbf{f}_{g_{2}})$$

which is rearranged into the equation in (8).

The control toques (τ_R, τ_L, τ_A) necessary to specify motion of the wings and abdomen can then be obtained from (10) by substituting the integrated (g_1, ξ_1) .

4.2 Wing and Abdomen Kinematics

Since we are prescribing the second set of configuration in (7), it would be simpler to parameterize the trajectories of these variables. Consider the model utilized in Tejaswi et al. [2020] for the motion of the wing relative to the body. Let $f \in \mathbb{R}$ be the flapping frequency in Hz and $T = \frac{1}{f}$ be the corresponding time period in seconds.

• The flapping angle is parameterized as

$$\phi(t) = \frac{\phi_m}{\sin^{-1} \phi_K} \sin^{-1} (\phi_K \cos(2\pi f t)) + \phi_0, \quad (11)$$

where $\phi_m \in \mathbb{R}$ is the amplitude, $\phi_0 \in \mathbb{R}$ is the offset, and $0 < \phi_K \le 1$ determines waveform shape.

• The pitch angle is given by,

$$\theta(t) = \frac{\theta_m}{\tanh \theta_C} \tanh(\theta_C \sin(2\pi f t + \theta_a)) + \theta_0, \quad (12)$$

where $\theta_m \in \mathbb{R}$ is the amplitude of pitching, $\theta_0 \in \mathbb{R}$ is the offset, $\theta_C \in (0, \infty)$ determines the waveform, and $\theta_a \in (-\pi, \pi)$ describes the phase offset.

• Finally, the deviation angle is given by

$$\psi(t) = \psi_m \cos(2\pi \psi_N f t + \psi_a) + \psi_0, \qquad (13)$$

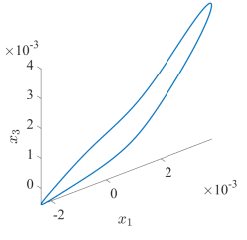
where $\psi_m \in \mathbb{R}$ is the amplitude, $\psi_0 \in \mathbb{R}$ is the offset, and the parameter $\psi_a \in (-\pi, \pi)$ is the phase offset.

Using these Euler angles, the attitude, angular velocity and acceleration of the wings can be constructed.

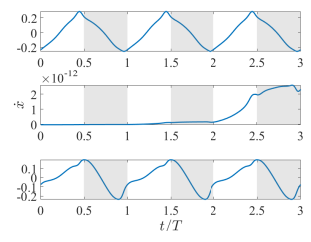
Next, the attitude of the abdomen relative to the body can be considered as $Q_A(t) = \exp(\theta_A(t)\hat{e}_2)$. This is motivated by the flight characteristics of a live Monarch butterfly which exhibits a nontrivial pitching motion of the abdomen (see Sridhar et al. [2020]). Here, the relative pitch angle is taken to be $\theta_A(t) = \theta_{A_m} \cos(2\pi f t + \theta_{A_a}) + \theta_{A_0}$, for fixed parameters $\theta_{A_m}, \theta_{A_a}, \theta_{A_0} \in \mathbb{R}$.

4.3 Periodic Motion

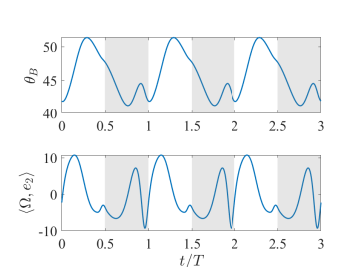
The above dynamic model yields the position and the attitude trajectory of the body for given kinematics of wings and abdomen. We first need to construct the kinematics of wings and abdomen for a particular maneuver. This is challenging due to the complexities of the dynamics



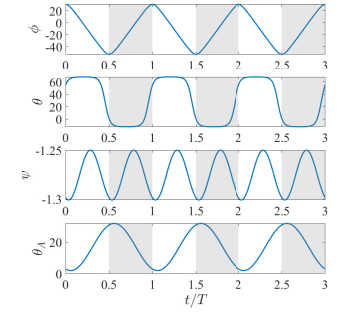
(a) Position of body x



(b) Velocity of body \dot{x}



gular velocity along 2nd axis



(c) Body pitch (in degrees) and an- (d) Prescribed wing kinematics and abdomen undulation (in degrees)

Fig. 2. Hovering periodic orbit generated using optimized parameters; shaded region corresponds to downstrokes

and the relatively large number of free parameters in the wing kinematics. Here we focus on the case of hovering flight, where the position and the attitude returns to the initial value after each flapping period. This result can be easily extended to other maneuvers such as forward flight or climbing.

This is addressed by a constrained optimization to minimize a performance index while ensuring that the motion is periodic. The parameters being optimized over characterize FWUAV wing kinematics and abdomen undulation along with the initial conditions. More specifically, this is formulated as follows.

• The objective function is

$$J = w_1 \int_0^T |E(t)| dt + w_2 \int_0^T |\dot{E}(t)| dt, \qquad (14)$$

where $w_1, w_2 \in \mathbb{R}$, and $E(t) = \frac{1}{2}m \|\dot{x}(t)\|^2 - mge_3^T x(t)$ is the sum of the kinetic energy and the gravitational potential energy. This is to minimize the variation of the energy while penalizing abrupt changes.

- The optimization parameters are given by
 - · flapping frequency: f and stroke plane angle: β
 - · wing kinematics: (ϕ_m, ϕ_K, ϕ_0) , $(\theta_m, \theta_C, \theta_0, \theta_a)$, (ψ_m,ψ_0,ψ_a)
 - · abdomen undulation : $(\theta_{A_m}, \theta_{A_0}, \theta_{A_a})$ · initial translational velocity: $\dot{x}(0) \in \mathbb{R}^3$

 - · initial attitude, angular velocity along 2nd axis: $\theta_B(0) \ s.t. \ R(0) = \exp(\theta_B(0)\hat{e}_2), \ \Omega_2(0) = \langle \Omega, e_2 \rangle$
- We ensure periodic motion by imposing the constraints: x(0) = x(T), $\dot{x}(0) = \dot{x}(T)$. Furthermore, there are additional constraints to avoid physically infeasible flapping, $|\phi_m| + |\phi_0| < \pi/2$, along with prescribed hard bounds on other parameters. It is

- also assumed that the motion of wings is symmetric to each other in this simple maneuver.
- The physical properties of the FWUAV including the wing morphological parameters like J_i, μ_i are taken to be similar to those of an actual Monarch. Their specific values are given in Sridhar et al. [2020].
- The aerodynamic properties including lift and drag coefficients are adopted from experimental data in Dickinson et al. [1999], Sane and Dickinson [2001]. Tejaswi et al. [2020] presents these expressions along with their relations to the actual aerodynamic forces and torques. Furthermore, aerodynamic forces due to the body and abdomen are ignored.

This problem is solved via global optimization techniques such as multistart in MATLAB. The corresponding optimized parameters are summarized in Table 1, and the resulting maneuver is illustrated in Figure 2. Note that since this maneuver is in the x-z plane, the relative attitude and angular velocity of the body are non-zero only along the y axis as shown in Figure 2.(c). Compared with Tejaswi et al. [2020] where the periodic orbit is constructed for the translational dynamics, this provides the periodic motion for the coupled translational and rotational motion in the higher-dimensional space.

Table 1. Optimized parameters

| Parameters | With abdomen | Without abdomen undulation | |
|------------------|--------------|----------------------------|--|
| | undulation | | |
| f | 11.7575 | 11.3975 | |
| β | -0.0087 | 0.2014 | |
| ϕ_m | 0.7271 | 0.6655 | |
| ϕ_K | 0.9493 | 0.0138 | |
| ϕ_0 | -0.1977 | -0.0434 | |
| θ_m | 0.6981 | 0.6980 | |
| θ_C | 2.8289 | 2.9968 | |
| θ_0 | 0.4843 | 0.3503 | |
| θ_a | 0.2905 | 0.3971 | |
| ψ_m | 0.0004 | 0.0003 | |
| ψ_N | 2 | 2 | |
| ψ_0 | -0.0223 | -0.0400 | |
| ψ_a | 2.7130 | 3.1109 | |
| θ_{A_m} | 0.2618 | | |
| θ_{A_0} | 0.2950 | 0.7667 | |
| θ_{A_a} | 2.7743 | | |
| $\dot{x}_{1}(0)$ | -0.2332 | -0.2437 | |
| $\dot{x}_{2}(0)$ | 0.0000 | 0.0000 | |
| $\dot{x}_3(0)$ | -0.0764 | -0.0859 | |
| $\theta_B(0)$ | 0.7314 | 0.5666 | |
| $\Omega_2(0)$ | -2.2583 | -0.1709 | |
| Optimized J | 0.0787 | 0.0890 | |

 $(f_{natural} = 10.2247 \,\mathrm{Hz}, \psi_N = 2)$

4.4 Effects of Abdomen

Now we study the influence of abdomen undulation on the periodic maneuver and the performance index. As a comparison, we identify another periodic orbit assuming that the abdomen is at a fixed relative attitude with respect to the body. The second column of Table 1 lists the optimized parameters wherein θ_{A_0} is the constant relative pitch of abdomen.

We observe that the objective function is decreased by about 12% when there is abdomen undulation when compared to no abdomen undulation. Since J in (14) is composed of energy and its derivative, they are also reduced

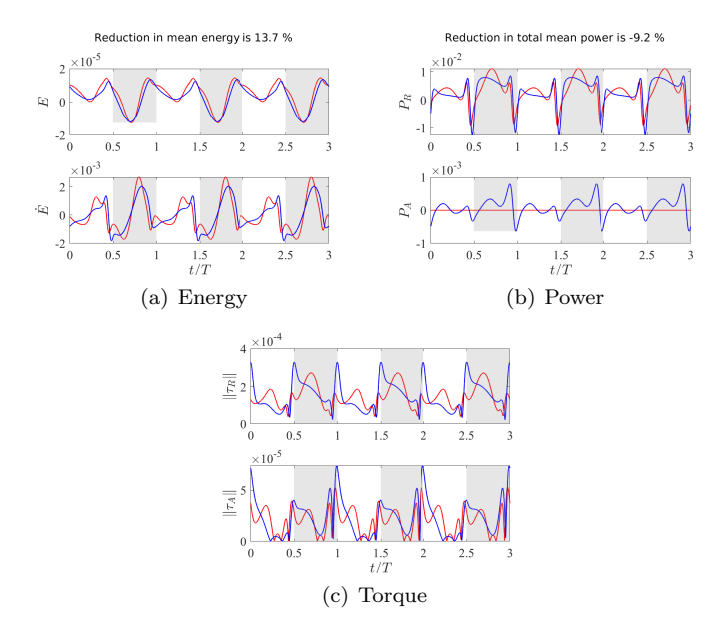


Fig. 3. Comparison between hovering with abdomen undulation (blue) and hovering without abdomen undulation (red)

in the case of abdomen undulation as seen in Figure 3.(a). This is not surprising as there are additional degrees of freedom that are utilized to minimize the objective function further.

Finally, the dynamical equations are utilized to obtain the control torques (τ_R, τ_L, τ_A) as shown in the proof of Proposition 7. For this numerical experiment, their magnitudes are illustrated at Figure 3.(c). Also, the power due to these external torques can be calculated as $P_R = \tau_R^T(Q_R\Omega_R)$ and $P_A = \tau_A^T(Q_A\Omega_A)$ in the body frame. Figure 3.(b) compares these values for the cases with and without abdomen undulation. Note that since the wings move symmetrically, $||\tau_R|| = ||\tau_L||$ and $P_R = P_L$.

4.5 Optimal Control

Now we formulate an optimal control problem such that an arbitrary trajectory asymptotically converges to the optimized periodic orbit for the hovering flight that we have obtained in the previous section. More specifically, let $\mathbf{x}(t) = (g_1(t), \xi_1(t)) = (x(t), R(t), \dot{x}(t), \Omega(t))$ represent the state of the FWUAV for the translational and rotational dynamics of the body. We have already obtained a periodic reference trajectory $\mathbf{x}_d(t) = (x_d(t), R_d(t), \dot{x}_d(t), \Omega_d(t))$. The objective is to adjust the control parameters such that $\mathbf{x}(t) \to \mathbf{x}_d(t)$.

We have various parameters in the definition of the wing kinematics in (11)–(13). Instead of numerically optimizing all of those parameters by brute-force, we identity a smaller set of parameters by investigating the effects of those on aerodynamic forces. So we choose $N_{\Delta}=6$ specific control parameters:

$$\Delta = [\Delta \phi_{m_s}, \Delta \theta_{0_s}, \Delta \phi_{m_k}, \Delta \phi_{0_s}, \Delta \theta_{0_k}, \Delta \psi_{0_k}].$$
 (15)

They are composed of two types:

- Symmetric parameters: for instance, $\Delta \phi_{m_s} = (\Delta \phi_{m,R} + \Delta \phi_{m,L})/2$ which is the average change of amplitude of the flapping angle of both wings
- Anti-symmetric parameters: e.g., $\Delta \phi_{m_k} = (\Delta \phi_{m,R} \Delta \phi_{m,L})/2$ which is the difference of flapping amplitude changes leading to a lateral force

Here, $\Delta \phi_{m,R} = \phi_{m,R}(t) - \phi_{m,R,d}$, i.e., the change of flapping amplitude of the right wing from the desired trajectory. Other variables are defined similarly. The effects of these control parameters on the resultant force and moment are summarized as follows. The proposed control

Table 2. Change in average forces/moments studied near the ideal hover trajectory

| | $\Delta \phi_{m_s}$ | $\Delta \theta_{0_s}$ | $\Delta \phi_{m_k}$ | $\Delta \phi_{0_s}$ | $\Delta \theta_{0_k}$ | $\Delta \psi_{0_k}$ |
|------------------------------------|---------------------|-----------------------|---------------------|---------------------|-----------------------|---------------------|
| $\Delta \bar{f}_{a_1} \times 10^4$ | -23 | -31 | 0 | -37 | 0 | 0 |
| $\Delta \bar{f}_{a_2} \times 10^4$ | 0 | 0 | 87 | 0 | -77 | 0 |
| $\Delta \bar{f}_{a_3} \times 10^4$ | -78 | 42 | 0 | 41 | 0 | 0 |
| $\Delta \bar{M}_{a_1} \times 10^5$ | 0 | 0 | 79 | 0 | 0 | 0 |
| $\Delta \bar{M}_{a_2} \times 10^5$ | -7 | 4 | 0 | 6 | 0 | 0 |
| $\Delta \bar{M}_{a_3} \times 10^5$ | 0 | 0 | -111 | 0 | 35 | -14 |

parameters improve the efficiency of optimization, and the corresponding optimized trajectories are more suitable to be generalized into other maneuvers.

To represent the variation of these control parameters over time, the flapping period [0,T] divided into $N_s=10$ steps at which the values of the control parameters are specified. Considering that the desired trajectory is periodic, we impose an additional constraint $\Delta(0)=\Delta(T)=0$. The value of $\Delta(t)$ between discrete steps are obtained by a piecewise linear interpolation.

The objective function is the weighted sum of the discrepancy between the desired trajectory and the controlled trajectory given by

$$J = \sum_{i=1}^{N_p} W_i \sqrt{\sum_j (W_{\mathbf{x}_j}(\mathbf{x}_j(t_i) - \mathbf{x}_{d_j}(t_i)))^2},$$
 (16)

where $t_i = i \times T/N_s$. The inner sum represents errors in the states \mathbf{x} at time t_i weighed by a factor $W_{\mathbf{x}_j}$. The outer sum combines the state errors over each prediction horizon N_p weighed by another factor W_i . The weighting factor for the state, $W_{\mathbf{x}}$ is designed to ensure that each component is scaled by its own physical characteristics. And the weighting factor for time, W_i gradually increases over i so that the terminal state error has more weight.

We follow the formulation of model predictive control, where the prediction horizon corresponds to two flapping period, i.e., $N_p=2N_s=20$. The optimization is repeated at every period to find the optimal control parameters over the prediction horizon, resulting in 120 optimal control parameters for two periods. Among those, the control parameters corresponding to the first period is actually implemented, and at the end of the period, optimization is repeated.

The initial states are taken to be

$$x(0) = \begin{bmatrix} -0.0003\\ 0.0004\\ -0.0004 \end{bmatrix}, \ R(0) = \begin{bmatrix} 0.7365 & 0.0163 & 0.6763\\ -0.0130 & 0.9999 & -0.0100\\ -0.6764 & -0.0014 & 0.7366 \end{bmatrix},$$

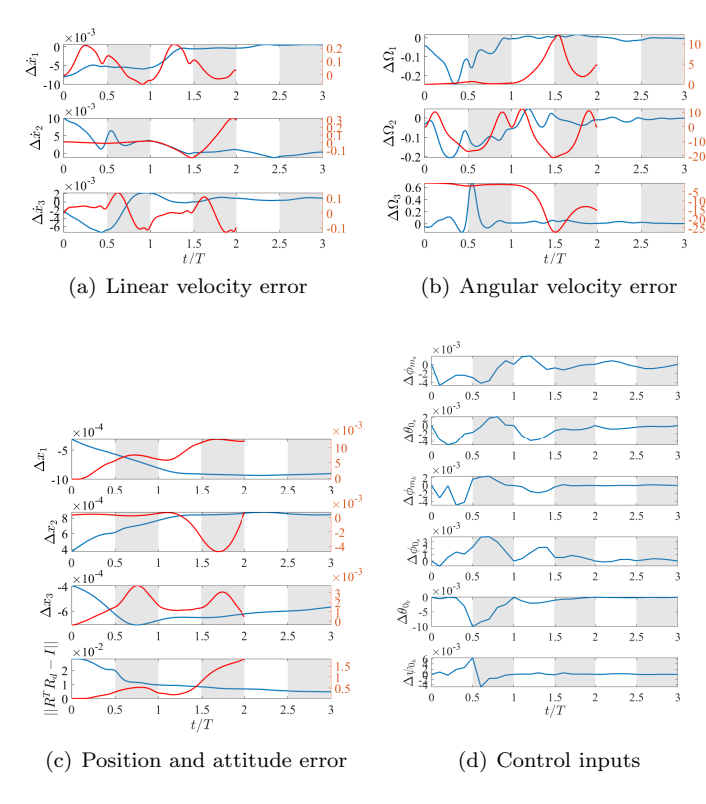


Fig. 4. Optimal trajectory errors in blue with scale on the left y-axis; uncontrolled trajectory errors in red with labels on the right y-axis

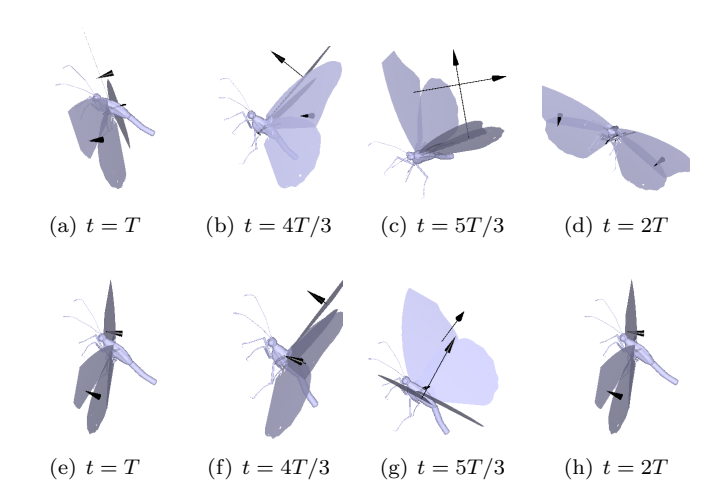


Fig. 5. Snapshots of flapping maneuver for hovering: uncontrolled trajectory in (a)-(d); controlled trajectory in (e)-(h) for the same initial condition

$$\dot{x}(0) = \begin{bmatrix} -0.2412\\ 0.0100\\ -0.0787 \end{bmatrix}, \quad \Omega(0) = \begin{bmatrix} -0.0437\\ -2.2907\\ -0.0487 \end{bmatrix}.$$

This optimization problem is numerically solved using fmincon in MATLAB. The resulting optimal trajectory errors and the snapshots are illustrated in Figure 4 and 5, with comparisons to another case without any control. It is shown that uncontrolled trajectories quickly diverge from the periodic orbit, whereas the controlled trajectories asymptotically converge to the hovering flight.

5. CONCLUSIONS

This paper presents an intrinsic formulation of a Lagrangian system on a Lie group, where the Lagrangian is composed of a configuration-dependent kinetic energy and a potential energy. This is utilized for the dynamics of a flapping-wing UAV inspired by Monarch butterfly. Two optimization problems are formulated to identify a periodic motion for hovering and also to stabilize it in the framework of model predictive controls. Future work includes constructing data-driven feedback control schemes by integrating a set of optimal trajectories computed by the proposed approach for varying initial conditions.

REFERENCES

Dickinson, M.H., Lehmann, F.O., and Sane, S.P. (1999). Wing rotation and the aerodynamic basis of insect flight. *Science*, 284(5422), 1954–1960.

Dyhr, J.P., Morgansen, K.A., Daniel, T.L., and Cowan, N.J. (2013). Flexible strategies for flight control: an active role for the abdomen. *Journal of Experimental Biology*, 216(9), 1523–1536.

Gibo, D.L. (1981). Altitudes Attained By Migrating Monarch Butterflies, Danaus P. Plexippus (Lepidoptera: Danainae), as Reported By Glider Pilots. *Canadian Journal of Zoology*, 59, 571–572.

Lee, T., Leok, M., and McClamroch, N. (2018). Global Formulation of Lagrangian and Hamiltonian Dynamics on Manifolds. Springer. doi:10.1007/978-3-319-56953-6.

Marsden, J. and Ratiu, T. (1999). Introduction to Mechanics and Symmetry, volume 17 of Texts in Applied Mathematics. Springer-Verlag, second edition.

Sane, S.P. and Dickinson, M.H. (2001). The control of flight force by a flapping wing: lift and drag production. *Journal of experimental biology*, 204(15), 2607–2626.

Shyy, W., Kang, C.k., Chirarattananon, P., Ravi, S., and Liu, H. (2016). Aerodynamics, sensing and control of insect-scale flapping-wing flight. Proceedings of the Royal Society A: Mathematical, Physical and Engineering Science, 472(2186), 20150712.

Sridhar, M., Kang, C.K., and Landrum, D.B. (2019). Beneficial effect of the coupled wing-body dynamics on power consumption in butterflies. In AIAA Scitech 2019 Forum, 0566.

Sridhar, M., Kang, C.K., and Lee, T. (2020). Geometric formulation for the dynamics of monarch butterfly with the effects of abdomen undulation. In *AIAA Scitech* 2020 Forum, 1962.

Tejaswi, K., Sridhar, M., Kang, C.K., and Lee, T. (2020). Effects of abdomen undulation in energy consumption and stability for monarch butterfly. *Bioinspiration & Biomimetics*.

Tejaswi, K. and Lee, T. (2021). Geometric Optimal Controls for Flapping Wing UAV on a Lie Group. In arXiv:2107.08008.

Xinyan Deng, Schenato, L., Wei Chung Wu, Sastry, S., Deng, X., Schenato, L., Wu, W.C., and Sastry, S. (2006). Flapping flight for biomimetic robotic insects: part I-system modeling. *IEEE Transactions on Robotics*, 22(4), 776–788.